ORIGINAL ARTICLE

Comparative mitochondrial proteomic analysis of human large cell lung cancer cell lines with different metastasis potential

Zhenkun Liu[1*], Song Xu[2*], Lu Li[1], Xiaorong Zhong[1], Chun Chen[2], Yaguang Fan[2], Wang Shen[2], Lingling Zu[2], Feng Xue[1], Min Wang[2] & Qinghua Zhou[1,2]

1 Lung Cancer Center/Lung Cancer Institute, West China Hospital, Sichuan University, Chengdu, China
2 Tianjin Key Laboratory of Lung Cancer Metastasis and Tumor Microenvironment, Tianjin Lung Cancer Institute, Tianjin Medical University General Hospital, Tianjin, China

Abstract

Background: Lung cancer is a highly aggressive cancer with a poor prognosis and is associated with distant metastasis; however, there are no clinically recognized biomarkers for the early diagnosis and prediction of lung cancer metastasis. We sought to identify the differential mitochondrial protein profiles and understand the molecular mechanisms governing lung cancer metastasis.

Methods: Mitochondrial proteomic analysis was performed to screen and identify the differential mitochondrial protein profiles between human large cell lung cancer cell lines with high (L-9981) and low (NL-9980) metastatic potential by two-dimensional differential gel electrophoresis. Western blot was used to validate the differential mitochondrial proteins from the two cells. Bioinformatic proteome analysis was performed using the Mascot search engine and messenger RNA expression of the 37 genes of the differential mitochondrial proteins were detected by real-time PCR.

Results: Two hundred and seventeen mitochondrial proteins were differentially expressed between L-9981 and NL-9980 cells ($P < 0.05$). Sixty-four analyzed proteins were identified by matrix-assisted laser desorption/ionization-time of flight mass spectrometry coupled with database interrogation. Ontology analysis revealed that these proteins were mainly involved in the regulation of translation, amino acid metabolism, tricarboxylic acid cycle, cancer invasion and metastasis, oxidative phosphorylation, intracellular signaling pathway, cell cycle, and apoptosis.

Conclusion: Our results suggest that the incorporation of more samples and new datasets will permit the definition of a collection of proteins as potential biomarkers for the prediction and diagnosis of lung cancer metastasis.

Introduction

Lung cancer is the leading cause of cancer-related death of both men and women worldwide.[1–9] Poor survival is associated with tumor metastasis.[10–15] Lung cancer metastasis is not only the malignant marker but is the main cause of treatment failure.[16–20] Metastasis is a complex

biological behavior that is correlated with many factors, genes, signal pathways, and biological processes.[21-26] Therefore, exploration of changes to molecular genetics and cell signal transduction related to invasion and metastasis in lung cancer will not only illuminate the molecular mechanisms of tumor invasion and metastasis, but also provide a new targeting molecule and route for blocking signal transduction and reversing the metastatic phenotype of lung cancer.[27-32] Our previous studies showed that low expression and hetero-deletion of tumor metastasis suppressor gene *nm23-H1* are closely correlated with high metastatic ability and poor prognosis in lung cancer patients.[25-34] We also demonstrated that transfection of wild type *nm23-H1* complementary DNA (cDNA) into human high-metastatic large cell lung cancer cells (which exhibit loss of heterozygosity [LOH] of *nm23-H1*), can regulate the expression of metastatic relative genes and reverse the metastatic phenotype of lung cancer cell lines.[23-30] Our findings and other reports have provided sufficient evidence to indicate that *nm23-H1* is a metastasis suppressor gene in many tumors.[21-37] Our studies have also proven that the *nm23-H1* gene is a key and upstream regulative gene in the "lung cancer metastatic suppressive cascade."[23-33] However, the exact molecular mechanism by which *nm23-H1* suppresses or reverses lung cancer metastasis is unclear.

Mitochondria are important organelles in cellular physiology. They have their own genomic system independent from the nucleus, and possess their own transcription, translation, and protein assembly machinery.[13,38-47] They are the principal suppliers of adenosine triphosphate, playing a central role in cellular energy metabolism and apoptosis. The oxidative metabolism of mitochondria contributes to harmful protein modifications, even under normal conditions.[39-41] Mitochondrial function changes have been implicated in tumor formation, including increased production of reactive oxygen species (ROS), decreased oxidative phosphorylation, and a corresponding increase in glycolysis.[13,41-43] Recently, deregulated cellular energetics have been considered an additional emerging hallmark of cancer.[13] Cancer cell signaling regulated by kinases and phosphatases is guided by cellular redox status and may be key in malignant transformation.

The protection of mitochondrial protein function is an important aspect of cellular protein quality control. However, mitochondrial proteins are difficult to characterize because of their relatively low abundance. Subcellular proteomic research would represent a significant advancement in the profiling of mitochondrial changes in diseased cells.[43] Two-dimensional differential in gel electrophoresis (2D-DIGE), coupled with matrix assisted laser desorption-ionization-time of flight (MALDI-TOF)

mass spectrometry (MS) has is frequently been applied in this field.[29,30,44] However, mitochondrial proteomic profiles in non-small cell lung cancer (NSCLC) remain poorly defined, particularly related to lung cancer metastasis. We conducted differential profiling of mitochondrial proteins from NSCLC cell lines with high and low metastatic potential and analyzed mitochondria-related metabolic pathways to identify the possible molecular markers of NSCLC metastasis.

Methods

Cell lines and reagents

A human high metastatic large cell lung cancer cell line (L9981) and low metastatic large cell lung cancer cell line (NL9980) were established from a human lung large cell carcinoma cell line (WCQH-9801) in our laboratory.[48] Cell lines were cultured in RMPI 1640 medium containing 10% fetal bovine serum (Gibco, Grand Island, NY, USA) at 37°C with 5% CO_2 incubator. Cy2, Cy3, and Cy5 were purchased from GE Healthcare (Piscataway, NJ, USA). Immobiline pH-gradient (IPG) DryStrips (pH 3–10,24 cm), IPG buffer (pH 3–10), DryStrip cover fluid, thiourea, urea, dithiothreitol (DTT) , Pharmalyte (pH 3-10), bromophenol blue, Commassie Brilliant Blue G-250, Tris base, sodium dodecyl sulfate (SDS), and molecular weight marker were purchased from Amersham Biosciences (Uppsala, Sweden).

Modified trypsin (sequencing grade) was obtained from Promega (Madison, IL, USA). Sucrose and mannitol were purchased from Sango (Shanghai, China). All analytical grade chemicals and biochemicals were prepared with Milli-Q deionized water (Millipore, Bedford, MA, USA).

Primary anti-fumarate hydratase (sc-27995), PRDX3 (sc-23969), HSP75 (TR1) (sc-13557), ERAB (sc-58525), PCNA (sc-56), and cytochrome c (SC-13560) antibodies were purchased from Santa Cruz Biotechnology (Santa Cruz, CA, USA), and anti-PHB (#2426) and COX IV (#4844) antibodies were purchased from Cell Signaling Technology (Danvers, MA, USA).

Isolation and purification of mitochondria

Cells were collected by centrifugation at 700 g for 10 minutes and the pellets were resuspended in homogenization medium A (20 mM Hepes-KOH, 1 mM ethylene-diamine-tetraacetic acid [EDTA], 1 mM phenylmethylsulfonyl fluoride [PMSF], 50 mM sucrose, 200 mM mannitol, pH7.4). The suspension was left on ice for 10 minutes. Cells were then dounce-homogenized and the lysis was monitored for quality by using phase-contrast microscopy until at least

90% of the cells were broken. The homogenate was centrifuged at 1000g for 10 minutes at 4°C and supernatant A was collected. The pellets were then washed twice with homogenization Medium B (20 mM Hepes-KOH, 25 mM KCl, 5 mM MgCl₂, 1 mM PMSF, 250 mM sucrose, pH7.4), and saved as the nuclear fraction. Supernatant A was centrifuged at 12 500g for 15 minutes at 4°C, and the pellet was collected and then washed once as a heavy membrane pellet. The heavy membrane pellet was resuspended in homogenization Medium A and spun again at 4000 g for 15 minutes to obtain the heavy mitochondrial pellet.

The heavy mitochondrial pellet was overlaid on a sucrose step density gradient (1.0 M sucrose over 1.5 M sucrose in 10 mM Tris_HCl [pH 7.4], 1 mM EDTA). The preparation was ultracentrifuged at 60 000 g for 20 minutes at 4°C to obtain mitochondria-enriched pellets. The pellets were washed twice in homogenization medium A.

Sodium dodecyl sulfate-polyacrylamide gel electrophoresis

The mitochondria-enriched pellets were suspended in the loading buffer (50 mM Tris-HCl, pH 6.8, 100 mM DTT, 2% SDS, 0.1% bromophenol blue, 10% glycerol) and run on SDS-polyacrylamide gel electrophoresis (PAGE, T = 12%) in Tris-glycine running buffer with 50 ug of protein per lane.

Western blot analysis

The mitochondria proteins were transferred to nitrocellulose membrane (Amersham Biosciences) under wet conditions at 80 V for two hours. Blots were blocked with blocking buffer (20 mM Tris-HCl, pH 7.5, 150 mM NaCl, 0.05% Tween-20, 5% nonfat dried milk) for one hour at room temperature. Different organelle marker protein antibodies and other primary antibodies were then added and the proteins were incubated overnight at 4°C. The blot was washed with TBST (20 mM Tris-HCl, 150 mM NaCl, 0.05% Tween-20, pH 7.5). The films were scanned using the Powerlook scanner (UMAX Technologies, Dallas, TX, USA) and quantified by Image Quant software (TL 7.0).

Two-dimensional differential in gel electrophoresis of mitochondria proteins

The mitochondria-enriched pellets were dissolved in lysis buffer (7 M urea, 2 M thiourea, 4% 3-((3-cholamidopropyl) dimethylammonio)-1-propanesulfonate [CHAPS], 30 mM Tris, 1 mM PMSF, pH8.5) at 4°C for one hour with intermittent sonication and then centrifuged at 20 000g for 30 minutes at 4°C. Protein extracts were purified using the Ettan 2D CleanUp kit (Amersham Biosciences) according to manufacturer's instructions, and adjusted to pH 8.5. The concentration of the total proteins was measured by using a 2D Quant kit (Amersham Biosciences).

The mitochondria protein lysates from two cell lines were labeled with Cy2, Cy3, and Cy5 following the protocols described in the Ettan DIGE User Manual (18-1164-40 Edition AA, GE Healthcare). Typically, 50 µg lysates were labeled with 400 pmol of Cy3 or Cy5, while the same amount of the pool standard of both samples was labeled with Cy2. We crossed fluorochromes between the pairs of analyzed samples to avoid differences resulting from the staining effectiveness. To achieve statistical confidence, three biological replicates were employed. Labeling reactions were carried out in the dark on ice for 30 minutes before quenching with 1 µL of 10 mM lysine for 10 minutes on ice. These labeled samples were then combined for 2D-DIGE analysis.

Cy3 and Cy5 labeled samples (50 µg) were combined before mixing with 50 µg Cy2 labeled internal standards. An equal volume of 2× sample buffer (7 M urea, 2 M thiourea, 4% CHAPS, 30 mM Tris, 1 mM PMSF, 130 mM DTT, 2% IPG buffer) was added to the sample and the total volume was made up to 450 µL with rehydration buffer (7 M urea, 2 M thiourea, 2% CHAPS, 15 mM DTT, 0.5% IPG buffer). The proteins were applied to IPG strips (pH 3-10, linear, 24 cm) and focused on an IPGphorIII (Amersham Biosciences) for a total of 64 kVH. The focused IPG strips were equilibrated and then applied to 12.5% SDS-PAGE using low-fluorescence glass plates on an Ettan DALT SIX system (Amersham Biosciences). All electrophoresis procedures were performed in the dark. After SDS-PAGE, the gels were scanned on a Typhoon 9400 scanner (GE Healthcare) at appropriate excitation/emission wavelengths specific for Cy2 (488/520 nm), Cy3 (532/580 nm), and Cy5 (633/670 nm) to generate spot maps. We prepared another strip in parallel as a preparative gel for spot pickings using the same process, except the IPG strip was loaded with 1000 µg proteins and the gel was stained with Coomassie brilliant blue.

Imaging analysis

DeCyder 6.5 software was used for 2D-DIGE analysis, according to the manufacturer's recommendations. The DeCyder differential in-gel analysis (DIA) module was used to compare each cell line mitochondria protein sample to the internal standard in each gel. The DeCyder biological variation analysis module was then used to simultaneously match all spot maps, using Cy3: Cy2 and Cy5: Cy2 DIA ratios, to calculate average abundance

changes and Student's *t*-test *P* values for the variance of these ratios for each protein across all samples. The differential protein spots (|ratio|NL9980/L9981 ≥ 1.2, *P* ≤ 0.05) were selected for identification.

Protein identification by mass spectrometry (MS)

Spots of interest were chosen using an Ettan Spot Picker from the preparative gel, destained, and digested with in-gel trypsin. Tryptic peptides (0.5 μL) were mixed with 0.5 μL matrix solution (α-cyano-4-hydroxycinnamic acid [CHCA] in 50% acetonitrile

[ACN]/0.1% trifluoroacetic acid [TFA]) and then analyzed using an AutoFlex MALDI-TOF/TOF mass spectrometer with LIFT technology (Bruker Daltonics, Bremen, Germany) to obtain the peptide mass fingerprint. Peptide matching and protein searches against the NCBInr database were performed using the Mascot search engine (http://www.matrixscience.com/) with a mass tolerance of ±100 ppm.

Functional enrichment analyses of mitochondrial differential proteins and protein–protein interaction data

The gene names of mitochondrial differential expression proteins were converted to NCBI-Entrez format for consistency and saved as a text file that was input into Cytoscape version 3.0.2 (www.cytoscape.org), BiNGO plugin 3.0.2, and AgilentLiteratureSearch 3.0.3.beta downloaded from Cytoscape manage plugin was used to analyze the enriched biological processes, molecular functions, and literature based protein–protein interaction network studies.

RNA isolation, reverse transcription reaction, and real-time PCR

Total cellular RNA was isolated from 5×10^6 cells using the Trizol reagent (Invitrogen, Carlsbad, CA, USA) according to the manufacturer's instructions, and quantified using an ultraviolet spectrophotometer (Beckman Coulter, Fullerton, CA, USA).

RNA (2 μg) was reverse transcribed using an M-MLV Reverse Transcriptase Kit (Promega) according to the manufacturer's protocol. Resultant cDNA (20 ng) was mixed with SYBR Green Master Mix (Applied Biosystems by Life Technologies, Foster City, CA, USA) and interest genes primer and amplified in the ABI7500 Real-time PCR System according to the manufacturer's protocol. The results of relative quantification were analyzed by comparison of $2^{-\text{average}\Delta\Delta C_T} \times 100\%$. The PCR primers are shown in Table 1.

Statistical analysis

Data are presented as means ± standard deviation and the *t*-test was used to analyze the differences between NL9980 and L9981 cell lines. *P* < 0.05 was considered statistically significant. PCR and Western Blot analyses were repeated at least three times.

Results

Enrichment of mitochondrial fractions

After protein extraction, we performed Western Blot analysis using cytochrome c, a mitochondrial marker, and PCNA, a nuclear marker. Cytochrome c was enriched while PCNA was barely detectable in the mitochondrial fraction, indicating that mitochondrial enrichment was not contaminated by proteins from other subcellular compartments (Fig 1).

Identification of differential proteins by MS

The mitochondria proteins of NL9980 and L9981 cell lines were compared by DIGE analysis and the mean number of spots detected in the three gels was 2333 ± 96.2 (Fig 2). Among 1722 ± 311.1 matched protein spots, 217 spots were differentially expressed in NL9980 and L9981 cell lines (|ratio| NL9980/L9981 ≥ 1.2). Sixty-four protein spots with the most remarkable alteration were further analyzed by MALDI-TOF peptide fingerprint and their molecular functions were summarized (Table 2).

Functional enrichment analyses of mitochondrial differential proteins and protein–protein interaction data

Functional enrichment category analyses of mitochondrial differential proteins were identified. The functional enrichment maps of the biological process and molecular function are shown in Figures 3 and 4, respectively. The white color shows non-significance in enrichment analysis; the color range from yellow to orange shows an adjusted *P* value from 0.05 to < 5*10-7. The statistical significantly enriched biological processes and molecular functions (*P* < 0.05, adjusted using the Bonferroni correction) are listed in Table 3. Biological processes, such as cellular respiration, energy derivation by oxidation of organic compounds, electron transport chain, respiratory electron transport chain, cellular metabolic process, generation of precursor metabolites and energy, oxidation reduction, and the metabolic process were enriched. Molecular functions,

Table 1 Primers of real-time PCR analysis

Protein ID	Gene symbol	Forward Primer	Reverse Primer
1405	CAMSAP1	ATATGCTGTATGCGCCATTAGTG	GGGCTGAACAAAATCTGGCTT
1451	MRPL1	GGAAGGCGAACCTGAGGATG	TGCCATATCCAGTGTCAAATCAA
917	GLS	CACTCAAATCTACAGGATTGCGA	CTCCAGACTGCTTTTTAGCACTT
1526	ATPAF1	TCAAATGTGTGGAACAGAAGACA	TGCGTAGACTGTATCTTTTGCTG
799	ME 2	CTCTGTAACACCCGGCATATTAG	GGTGGGTAAAGTCTCCCTTGG
1685	FAM82B	TCAGTTGCTAACCCAATACAAGG	CTCTTCTGAGGTTCTGCTAAGC
1088	PDHA1	TCGCAGAGCTTACAGGACGA	ACTTACAGGCTAGAGCAATCCC
1172	ACADM	GGAGATCACAGCATACAAAAGCC	TTAGGGGGACTGGATATTCACC
1594	ABHD11	TCCGCTTTCCTACAGGCTTCT	GAAGAGCCCGTGCAAAAAGA
1678	HSD17B10	AAGAAGTTAGGAAACAACTGCGT	CAGGCGGATCACATTGAAGGT
1095	UQCRC1	CGGTGGGAGTGTGGATTGATG	GCCGATTCTTTGTTCCCTTGA
923	DLD	GAAATGTCCGAAGTTCGCTTGA	TCAGCTTTCGTAGCAGTGACT
923	SAMM50	CAAGTGGACCTGATTTTGGAGG	AGACGGAGCAATTTTTCACGG
1563	COQ5	AGAGCTGGACTTGCATGGGTA	GGGGATTGTTCACTTGGCTAAAT
1356	MRPL39	CCGACAGAATTGACAGAAATGCG	CTTCTCAGTTCGGGGAGTTAATG
1606	AK2B	AAGCCTACCACACTCAAACCA	GCTTGCGAACACGACATCG
740	MIPEP	TCTTACCAGAACACATTCGTCG	CTGCTGCTGAGCAATTCTTCTA
1664	APOA1BP	GTGTCCTGAAGGGACTCACTG	CCCAGGTAATGGTAGCGACC
1916	NDUFA5	AGGAAATCCCTAAAAATGCAGCA	TCTTCCACTAATGGCTCCCATA
1660	UQCRFS1	TGCTTCTGTTTGTTATTCCCACA	AAACCTTTCCTAGCCTCGCTG
1169	MRPL38	AACAGTGACATCGACTTGAGC	CCCGAAATACTCTCGGTAGGTC
1301	TIMM50	GACGAAAATGGTGCCAAGAT	TAGGGTGGCTGGTAGTACGG
1093	FH	ATGGTCTTGATCCAAAGATTGCT	TGATCCAGTCTGCCATACCAC
1138	CS	CCATCCACAGTGACCATGAG	CTTTGCCAACTTCCTTCTGC
1665	NDUFS3	ACTGTCAGACCACGGAATGAT	CCCTGAGGAAAGTCAGCACTG
1932	ATP5J	GTTCTCCTCTGTCATTCGGTCA	CCAGCTCTTGCTGATACTCTGAA
1553	PHB	GGCTGAGCAACAGAAAAAGG	GCTGGCAGGTAGGTGATGTT
1586	AK2a	TGCAAGCCTACCACACTCAAA	GACATCGGGGGTCTGGGAT
962	LAP3	CACACGTTTAACCCGAAGGT	AGAGAGGCATCCTCCAGACA
1227	CECR5	CCACAGAGTGATCCCTGCTG	CGCTTCTCATGGTACTCGGA
1589	DCI PROTEIN	AACCCCAGGTACTGCATAGGA	CAACCAGAAAGGGGCGATGAT
1296	Coprox	AAGGCTGGGGTGAGCATTTC	GATTCTTGGGGTGGATAACAGAG
971	ALDH7A1	TGGGCAGATATTCCTGCTCCA	CCCACACCTTCCACTAAGATTTT
1717	PRDX3	GCCGTTGTCAATGGAGAGTTC	GCAAGATGGCTAAAGTGGGAA
1139	NDUFS2	GGAGTCCGATTGCCGATTCAG	GGGCTGTTTCTTTGCTTGGG
709	GPD2	TGAACCTGGCCTATGTTAAAGC	GGCTGTTTTTAGTCCTCTGGTG
1756	SOD2	AACCTCAGCCCTAACGGTG	AGCAGCAATTTGTAAGTGTCCC
Endogenous gene	GAPDH	AGCCGAGCCACATCGCT	GGCAACAATATCCACTTTACCAGAGT

GAPDH, glyceraldehyde 3-phosphate dehydrogenase.

such as oxidoreductase and catalytic activity, were also enriched. The results showed that most of enriched proteins of the identified mitochondrial differential proteins were oxidoreduction-related proteins and biological processes were oxidoreduction-related processes.

A literature based protein–protein interaction subnetwork of mitochondrial differential proteins was generated using AgilentLiteratureSearch from CytoScape. The results are shown in Figure 5. In this subnetwork, the colored circles (nodes) represent proteins, the yellow circles represent the proteins from our results, and the grey full lines (edges) represent protein–protein interactions. Mitochondrial differential proteins, such as PRDX3, SOD2,

PHB, HSP75 (TRAP1) and GLS, more frequently interacted with other proteins. These interaction data provide important insight into the molecular mechanisms of NSCLC metastasis.

Validation of differentially expressed proteins on gene level by real-time PCR

To verify the 2D-DIGE profiling results, we selected 37 genes and detected their expression by real time PCR. The genetic alterations of selected mitochondria proteins conformed to the 2D-DIGE data (Fig 6).
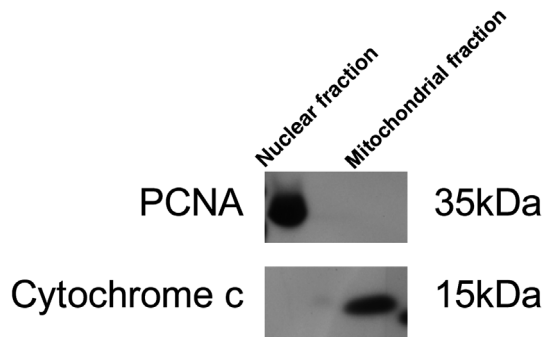
Figure 1 Representative Western blot analysis of mitochondria-enriched fraction. PCNA was used as a nuclear marker and cytochrome c as a mitochondrial marker. Proteins (50 μg) were loaded per lane and detection was performed using electrochemiluminescence.

Validation of differentially expressed proteins by Western blotting

To further validate the 2D-DIGE profiling result from protein level, we performed Western blot analysis on several interesting mitochondrial proteins, including FH, PRDX3, HSP75, ERAB, and PHB. The expression of recruited proteins was significantly higher in NL9980 cells compared to

L9981 cells, which was consistent with results from the 2D-DIGE data (Fig 7).

Discussion

To a large extent, the poor prognosis of lung cancer is associated with its malignant metastatic phenotype. To better explore and understand the mechanism of lung cancer metastasis and to search for potential markers for early diagnosis and reverse metastasis, we previously performed differential proteomic analysis in two human large cell lung cancer cell lines with high (L9981) and low (NL9980) metastasis potential by 2D-DIGE. The data suggest that obvious differential proteomic expression exists between human high and low metastatic large cell lung cancer cell lines.[44] Although the molecular mechanisms have gradually been deciphered, the function of mitochondria in the process of lung cancer metastasis remains unknown. Some studies have demonstrated that in certain tumors, such as nasopharyngeal and hepatocellular carcinoma, mitochondrial proteins are the potential biomarkers for cancer initiation and progression.[45–47] Therefore, we proposed that mitochondrial proteins might be differentially expressed in lung cancer metastasis.
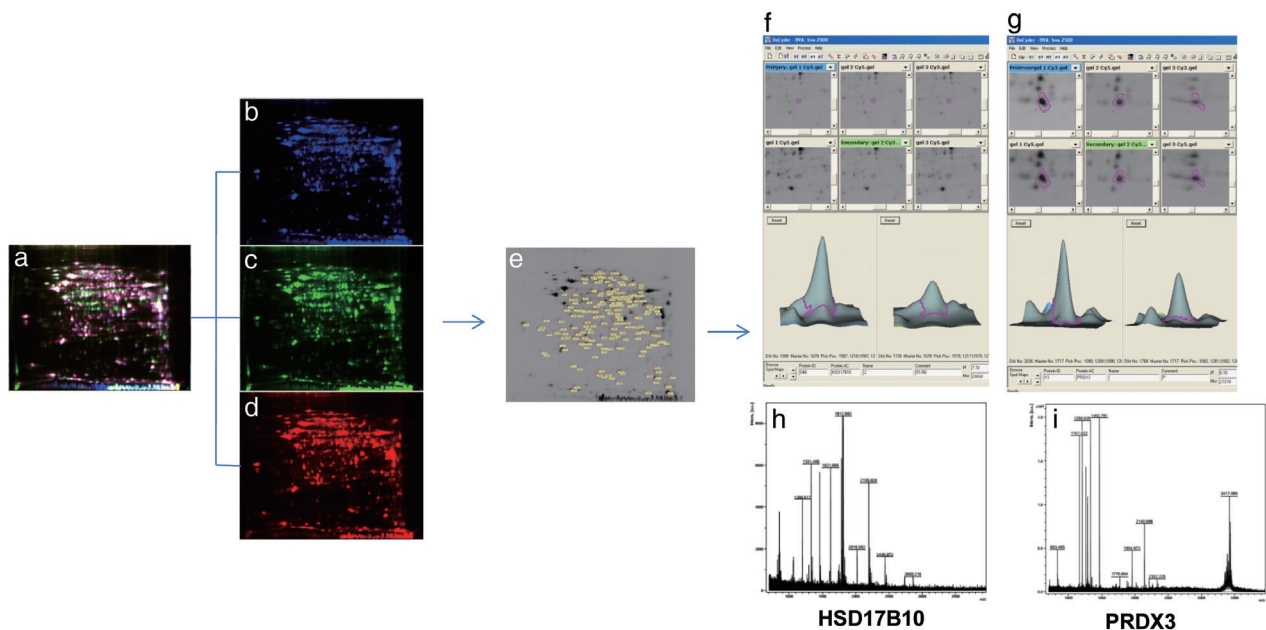

Figure 2 Differential expression of mitochondrial proteins in NL9980 and L9981 cell lines. (**a–d**) DeCyder software output of typical two-dimensional differential in gel electrophoresis images of the mitochondrial proteins in NL9980 and L9981 cell lines; the protein lysates are labeled with either Cy3 (green) or Cy5 (red), respectively. (**e**) Identification of differentially expressed proteins. (**f–g**) Three-dimensional images of HSD17B10 and PRDX3, which show that HSD17B10 and PRDX3 levels are higher in NL9980 compared to L9981 cell lines (**f**) Results of matrix assisted laser desorption-ionization-time of flight mass spectrometry analysis of protein spots of HSD17B10 and PRDX3 by peptide mass fingerprinting analysis.

Table 2 Differentially expressed mitochondria proteins between NL9980 and L9981, identified by mass spectrometry

Master No.	Accession No.	t-test	Av. Ratio	Protein name	Reported molecular function	Calculated PI value	Nominal mass (Mr)	Sequence covered (%)	Score
625	gi|5822580	0.00074	−10.41	Chain A, crystal structure of the human Pax-6 Paired domain-DNA complex reveals a general model for Pax protein-DNA interactions		9.86	14 744	45	66
1405	gi|186659512	0.00016	−8.63	CAMSAP1	Cytoskeleton organization	6.28	179 230	6	67
1423	gi|83405782	0.000085	−7.35	VEPH1		6.28	90 436	9	66
1339	gi|4324699	0.00019	−7.25	NUMA1	Structural molecule activity, lung epithelial cell differentiation	10.56	31 952	37	68
1324	gi|4457970	0.000085	−7.01	tn88b03.x1 NCL_CGAP_Ut2 *Homo sapiens* cDNA clone IMAGE:2176589 3', mRNA sequence		9.46	10 934	60	92
1490	gi|77939099	0.0012	−6.53	MCF7RNAL18G24TF Human MCF7 breast cancer cell line near full length normalized library (MCF7_EST) Homo sapiens cDNA clone MCF7_RNA_L_18_G24 mRNA sequence		5.44	19 514	34	92
1424	gi|55666319	0.00024	−6.41	CASK (MAGUK family)	Glycogen biosynthetic process, protein amino acid phosphorylation, intracellular protein transport, cell adhesion	5.83	67 245	18	74
1831	gi|5454090	0.0038	−6.37	SSR4	Intracellular protein transport	5.76	19 158	35	111
1170	gi|77935996	0.000097	−6.32	MCF7RNAL16B02TR Human MCF7 breast cancer cell line near full length normalized library (MCF7_EST) Homo sapiens cDNA clone MCF7_RNA_L_16_B02, mRNA sequence		6.17	23 959	42	122
1036	gi|76827262	0.000097	−6.1	ETV2	Regulation of transcription, DNA-dependent	9.16	17 837	30	67
1420	gi|34536332	0.000097	−5.54	GFAP	Structural constituent of cytoskeleton	5.84	49 533	12	54
1420	gi|34782991	0.000097	−5.54	INPP5B	Signal transduction, microtubule cytoskeleton, metal ion binding	5.44	85 202	8	54
1451	gi|74733472	0.00099	−4.16	MRPL1	Translation, RNA binding, structural constituent of ribosome	8.19	34 602	27	78
1629	gi|49119653	0.00049	−1.67	YWHAZ	Protein targeting mitochondrion, anti-apoptosis, signal transduction	4.72	30 100	38	100
1343	gi|13786630	0.017	−1.58	Chain A, crystallographic structure of human branched chain amino acid aminotransferase (mitochondrial) complexed with PLP at 1.95 angstroms (orthorhombic form)	Valine, leucine, and isoleucine degradation and biosynthesis, pantothenate and CoA biosynthesis	8.48	41 635	29	94
685	gi|18677024	0.01	−1.24	PDE2		6.33	59 567	31	87
685	gi|50513540	0.01	−1.24	Chain A, Moesin FERM domain bound to EBP50 C-terminal peptide	Regulation of lymphocyte migration	9.03	35 010	32	75
917	gi|6002671	0.00084	3.82	GAC	Glutamine metabolic process	6.05	58 678	17	98
1431	gi|21361454	0.00032	3.25	PYCR2	Amino acid biosynthetic process, electron transport	7.66	33 958	35	116

Table 2 Continued

Master No.	Accession No.	Av. Ratio	t-test	Protein name	Reported molecular function	Calculated PI value	Nominal mass (Mr)	Sequence covered (%)	Score
670	gi|14149738	2.8	0.0032	Neurolysin	Proteolysis	6.21	81 341	40	200
1526	gi|110349780	2.58	0.0012	ATPAF1 isoform 1 precursor		8.12	36 756	33	180
799	gi|4505145	2.54	0.00033	ME2, NAD(+)-dependent, mitochondrial	Malate metabolic process, metabolic process	7.53	66 029	37	166
1434	gi|74733472	2.45	0.00026	MRPL1	Translation, RNA binding, structural constituent of ribosome	8.19	34 602	33	84
580	gi|46249758	2.39	0.00026	Ezrin	Epithelial cell differentiation, actin filament binding	5.94	69 313	28	154
1685	gi|119612044	2.39	0.0045	FAM82B, isoform CRA_a	Binding	6.21	31 180	20	70
1088	gi|62897039	2.36	0.00085	PDC (lipoamide) alpha 1 variant	Acetyl-CoA metabolic process, glycolysis, metabolic process	8.35	43 934	40	130
1088	gi|119572383	2.36	0.00085	TUFM-1, isoform CRA_b	Cell proliferation, mitochondria translation	6.14	37 775	26	54
1172	gi|4557231	2.19	0.00088	ACAD C-4 to C-12 straight chain isoform, a precursor	Electron transport, lipid metabolic process	8.61	47 015	44	198
1594	gi|40226380	2.19	0.00024	ABHD11	Proteolysis, aromatic compound metabolic process	9.24	34 310	28	115
1678	gi|83715985	2.12	0.000097	HSD17B10 isoform 2	Lipid metabolic, metabolic, enterobactin biosynthetic, and cellular metabolic processes	6.73	26 196	67	142
1095	gi|46593007	2.09	0.00029	UQCRC1	Electron transport, oxidative phosphorylation, proteolysis, transport, aerobic respiration	5.94	53 297	35	118
923	gi|62088 986	2.04	0.001	DLD, variant	Electron transport, transfer RNA processing, cell redox homeostasis	8.71	56 129	22	99
923	gi|14043738	2.04	0.001	SAMM50	Biological process	6.44	52 271	39	133
1563	gi|116063536	2.02	0.00049	COQ5	Ubiquinone biosynthetic process, metabolic process	6.47	37 402	45	152
736	gi|62089196	1.96	0.0076	TRAP1	Protein targeting	8.32	80 228	27	123
1356	gi|33337737	1.91	0.0024	MRPL39	TRAP1 variant	8.00	38 695	32	138
709	gi|119631857	1.91	0.00085	GPD2 (mitochondrial), isoform CRA_a	Glucose catabolic process, glycerol-3-phosphate metabolic process, gluconeogenesis, electron transport, insulinoma, non-insulin-dependent diabetes mellitus	7.23	79 202	23	97
1606	gi|7524346	1.89	0.0001	AK2 isoform b	Nucleobase, nucleoside, nucleotide, and nucleic acid metabolic process	7.71	25 769	43	127
740	gi|156105687	1.88	0.0012	MIP	Proteolysis, mitochondrial protein processing	6.6	81 357	19	80
1664	gi|119573328	1.88	0.0017	APOA1 isoform CRA_c	Biological process	5.27	26 369	46	118

Table 2 Continued

Master No.	Accession No.	t-test	Av. Ratio	Protein name	Reported molecular function	Calculated PI value	Nominal mass (Mr)	Sequence covered (%)	Score
1302	gi|46593007	0.0013	1.86	UQCRC1	Electron transport, oxidative phosphorylation, proteolysis, transport, aerobic respiration	5.94	53 297	42	166
1916	gi|4826848	0.00018	1.86	NDUFA5	Electron transport, mitochondrial electron transport, NADH to ubiquinone	5.75	13 507	42	124
1660	gi|45768728	0.000097	1.85	UQCRFS1	Electron transport, transport	8.55	29 958	29	112
1169	gi|15342081	0.00032	1.84	MRPL38		6.2	41 017	52	200
572	gi|4505257	0.00037	1.79	Moesin	Cell motility	6.08	67 892	29	100
1589	gi|16307101	0.0025	1.69	DCI	Lipid metabolism	6.32	27 250	32	114
1301	gi|14290586	0.00024	1.69	TIMM50	Protein amino acid dephosphorylation, mitochondrial membrane organization and biogenesis, protein transport, intracellular protein transport across a membrane	8.56	39 014	38	190
1093	gi|19743875	0.00055	1.66	FH precursor	Tricarboxylic acid cycle, fumarate metabolic process, cell cycle, negative regulation of progression, homeostasis of number of cells within a tissue through cell cycle	8.85	54 773	33	158
1139	gi|4758786	0.00065	1.66	NDUFS2	Electron transport, mitochondrial electron transport, NADH to ubiquinone, response to oxidative stress	7.21	52 911	27	105
1138	gi|48257138	0.00091	1.65	Citrate synthase	Carbohydrate metabolic process, tricarboxylic acid cycle	6.49	45 758	18	82
1665	gi|5138999	0.0015	1.65	NADH-Ubiquinone reductase	Electron transport, mitochondrial electron transport, NADH to ubiquinone, oxygen and reactive oxygen, pathogenesis, induction of apoptosis species metabolic process	7.77	30 401	51	252
1932	gi|18644883	0.0036	1.65	ATP5PF, mitochondrial isoform a precursor	Generation of precursor metabolites and energy, ion transport, ATP synthesis-coupled proton transport, proton transport	9.52	12 580	54	94
1553	gi|4505773	0.0011	1.64	PHB	Regulation of progression through cell cycle, DNA replication, signal transduction, negative regulation of cell proliferation, negative regulation of transcription	5.57	29 843	41	162

Table 2 Continued

Master No.	Accession No.	t-test	Av. Ratio	Protein name	Reported molecular function	Calculated PI value	Nominal mass (Mr)	Sequence covered (%)	Score
1586	gi|4502013	0.000097	1.64	AK2 isoform A	Nucleobase, nucleoside, nucleotide, and nucleic acid metabolic process	7.67	26 689	35	104
1142	gi|704416	0.0081	1.62	EF-Tu	DNA/RNA/protein synthesis	7.7	49 851	3	37
971	gi|116241244	0.0007	1.61	ALDH7A1	Aldehyde dehydrogenase (NAD) activity, L-aminoadipate-semialdehyde dehydrogenase activity, oxidoreductase activity	6.44	55 845	25	73
1227	gi|21914862	0.00038	1.54	CECR5	3.33333E+13	6.43	43 845	41	129
1717	gi|119569781	0.00043	1.53	PRDX3, isoform CRA_a	Activation of NF-kappaB transcription factor	5.73	24 941	49	84
1296	gi|433888	0.0026	1.48	CPOX	Porphyrin and chlorophyll metabolism	6.68	40 847	53	238
986	gi|122065129	0.0057	1.4	ALDH3B1 (ALDH class 2)	Glycolysis/gluconeogenesis	6.36	57 658	24	133
962	gi|37588925	0.00079	1.39	LAP3	3.33333E+13	6.80	54 754	49	197
973	gi|119577249	0.019	1.31	SARS2, isoform CRA_b		8.80	61 018	33	123
973	gi|119595468	0.019	1.31	NARS2 (mitochondrial) (putative), isoform CRA_b		6.79	53 699	15	66
1756	gi|38503339	0.0018	1.26	SOD [Mn], mitochondrial	Superoxide dismutase activity, manganese superoxide dismutase activity, oxidoreductase activity, manganese ion binding, metal ion binding	6.86	22 304	43	93

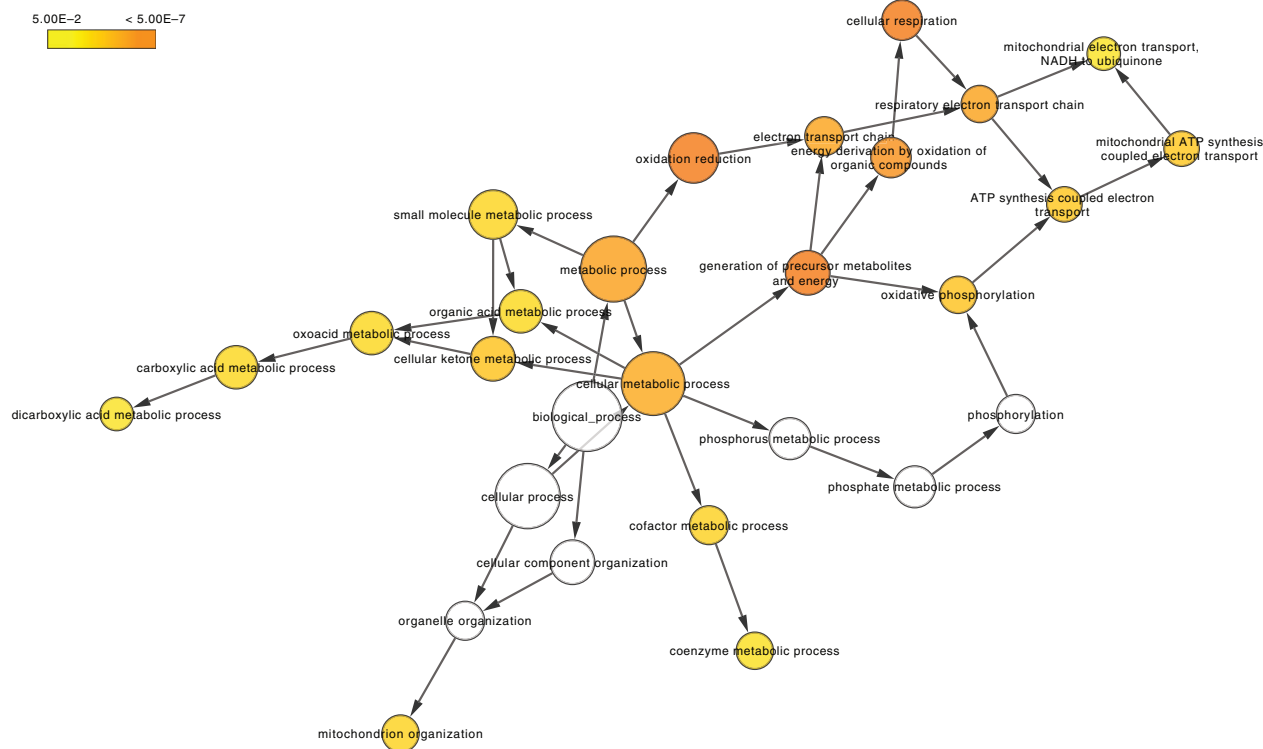*T*-test and Av. Ratio:NL9980/L9981.

Figure 3 Enriched biological processes of differentially expressed mitochondrial proteins between NL9980 and L9981 cell lines with low and high metastatic potential. Color circles represent biological processes, arrows represent the relationship between two biological processes, white circles show non-significance in enrichment analysis, and the color range from yellow to orange shows adjusted *P* values from 0.05 to < 5*10-7.

Routine protein analysis to detect mitochondrial proteins is difficult because of their low expression compared to non-mitochondrial proteins. In this study, we conducted 2D-DIGE analysis combined with MALDI-TOF/TOF to evaluate the differences in mitochondrial protein expression between two human large cell lung cancer cell lines with high (L9981) and low (NL9980) metastatic potential. Two dimensional-DIGE revealed 217 differential spots between the two cell lines, while MS revealed a further 64 spots with significant differences. Interestingly, a number of non-mitochondrial proteins that presented in the enriched mitochondria fraction were also differentially expressed between the two cell lines. These proteins are either peripherally associated with the mitochondria, sublocated in the mitochondria, or present as possible contaminants in the preparation. Nevertheless, according to Swiss-Prot annotation, the majority of the differentially expressed proteins were localized in the mitochondria. Among these candidates, six proteins piqued our interest, including FH, HSP75, ERAB, PHB, and PRDX3, which have previously been reported to be involved in cancer development and metastasis.

Loss-of-function of FH, a metabolic tumor suppressor, is associated with hereditary leiomyomatosis and renal cell carcinoma.[49] Studies have shown that FH-deficient cancer is characterized by impaired oxidative phosphorylation and a metabolic shift to aerobic glycolysis, a form of metabolic reprogramming referred to as the Warburg effect. These changes represent multiple biochemical adaptations in the glucose and fatty acid metabolism that supports malignant proliferation.[50,51] To date, no reports have identified the relevance of FH in lung cancer development and metastasis; however, in our study, we observed that L9981 cells showed significantly low expression of FH compared to NL9980 cells. As FH is reported to be a metabolic tumor suppressor, we assumed that FH might negatively regulate lung cancer invasion and metastasis.

HSP75, also called tumor necrosis factor type 1 receptor-associated protein (TRAP-1), is another down-regulated mitochondrial protein with high metastatic ability in L9981 cells. HSP75 is a negative regulator of mitochondrial respiration that can modulate the balance between oxidative phosphorylation and aerobic glycolysis. The impact of HSP75 on mitochondrial respiration
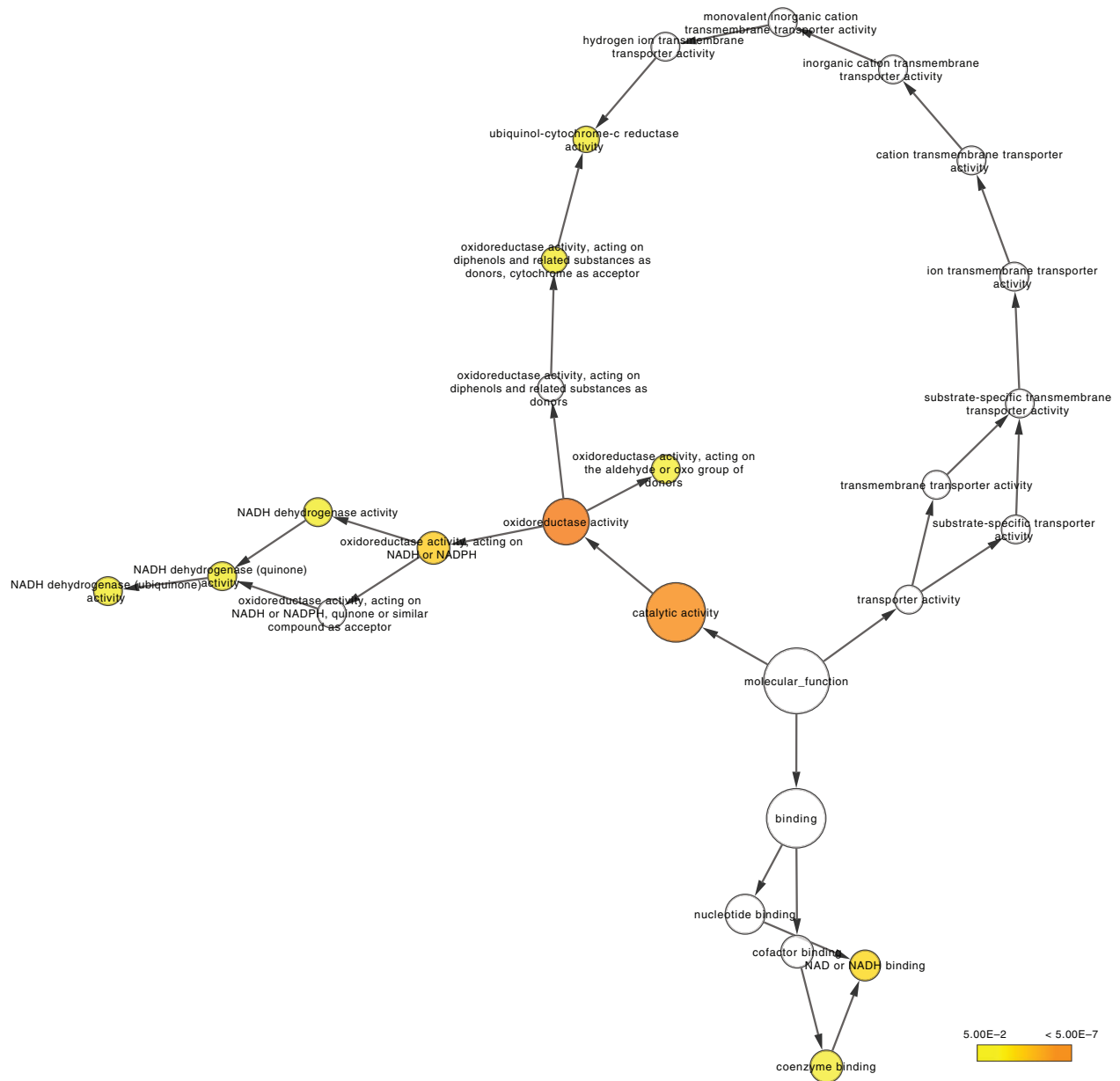
Figure 4 Enriched molecular functions of differentially expressed mitochondrial proteins between NL9980 and L9981 cell lines with low and high metastatic potential. Color circles represent molecular functions, arrows represent the relationship between two molecular functions, white circles show non-significance in enrichment analysis, and the color range from yellow to orange shows adjusted *P* values from 0.05 to < 5*10-7.

is probably mediated by the modulation of mitochondrial spare respiratory capacity (SRC) and the inhibition of *SDHA*. Previous studies have indicated that HSP75 expression is significantly reduced in bladder cancer and renal cell carcinoma compared to healthy tissues, but is increased in other types of tumors.[52–54] Recently, Agorreta *et al.* reported that HSP75 impacts the viability of NSCLC cells, and that its expression is prognostic in

NSCLC.[55] Liu *et al.* confirmed that HSP75 could stimulate the proliferation of lung cancer cells but inhibits metastatic spread.[56] However, Caino *et al.* reported contradictory findings, reporting that HSP75 favors metastatic dissemination in disease models in mice, and shortens overall survival in patients with NSCLC,[57] indicating that the role of HSP75 is complex in lung cancer metastasis.

Table 3 Functional enrichment category analyses of mitochondrial differential proteins

GO ID	GO term	*P*	Number of genes
Biological Process			
6732	Coenzyme metabolic process	2.75E-03	6
6082	Organic acid metabolic process	1.81E-03	10
45333	Cellular respiration	1.35E-07	8
7005	Mitochondrion organization	1.07E-03	6
15980	Energy derivation by oxidation of organic compounds	3.68E-06	8
22900	Electron transport chain	1.85E-05	7
22904	Respiratory electron transport chain	1.62E-05	6
19752	Carboxylic acid metabolic process	1.62E-03	10
42180	Cellular ketone metabolic process	2.25E-04	11
42773	ATP synthesis coupled electron transport	3.40E-04	5
43648	Dicarboxylic acid metabolic process	3.72E-03	4
44237	Cellular metabolic process	2.92E-05	31
51186	Cofactor metabolic process	9.28E-04	7
6091	Generation of precursor metabolites and energy	4.03E-07	11
44281	Small molecule metabolic process	1.31E-03	15
6119	Oxidative phosphorylation	2.45E-04	6
55114	Oxidation reduction	3.92E-09	16
43436	Oxoacid metabolic process	1.62E-03	10
42775	Mitochondrial ATP synthesis coupled electron transport	3.40E-04	5
8152	Metabolic process	1.31E-05	34
6120	Mitochondrial electron transport, NADH to ubiquinone	4.09E-03	4
Molecular Function			
51287	NAD or NADH binding	1.83E-03	4
16903	Oxidoreductase activity, acting on the aldehyde or oxo	2.10E-02	3
16681	Oxidoreductase activity, acting on diphenols and its analogues	4.35E-02	2
8137	NADH dehydrogenase (ubiquinone) activity	4.98E-02	3
8121	Ubiquinol-cytochrome-c reductase activity	4.35E-02	2
16491	Oxidoreductase activity	2.34E-09	16
3954	NADH dehydrogenase activity	4.98E-02	3
50136	NADH dehydrogenase (quinone) activity	4.98E-02	3
3824	Catalytic activity	2.55E-06	32
16651	Oxidoreductase activity, acting on NADH or NADPH	6.29E-04	5
50662	Coenzyme binding	2.65E-02	5

GO, gene ontology.

ERAB is characterized as a NAD +-dependent dehydrogenase that is constitutively expressed in tissues and overexpressed in neurons affected in Alzheimer's disease. Cells overexpressing ERAB in vitro are more sensitive to β-Amyloid-induced stress, and blocking ERAB activity has been shown to inhibit this cell death, indicating that β-Amyloid induced cell death is mediated by ERAB.[58,59] The role of ERAB in tumors has rarely been reported. The only study we located by Shen *et al.* indicated that ERAB is differentially expressed in HOXA13 knockdown esophageal squamous cell carcinoma cells.[60]

PHB is an evolutionary conserved protein that responds to mitochondrial stress and plays a role in regulating mitochondrial respiration activity.[61] It is considered a regulator of cell growth, proliferation, differentiation, aging, and apoptosis.[62] The role of PHB in cancer cell growth remains controversial. Many reports have shown evidence that PHB overexpression results in the inhibition of cancer cell growth, but the knockdown of PHB by small interfering RNA (siRNA) accelerates tumor growth in prostate, gastric, and liver cancers.[63–65] However, other studies have suggested that PHB plays a protumorigenic role. PHB is necessary for the activation of C-Raf by the oncogene Ras in HeLa cells.[66] In the present study, L9981 cells showed slightly decreased expression of PHB compared to NL9980 cells. The exact of role of PHB in lung cancer metastasis remains under investigation.

PRDX3 functions as an antioxidant and is localized in the mitochondrion. PRDX3 overexpression is associated with the cancer development, progression, and drug resistance. Results suggest that PRDX3 is upregulated in prostate cancer and plays an essential role in regulating oxidation-induced apoptosis in anti-androgen-resistant prostate cancer cells.[67,68] Moreover, PRDX3 is reported to be involved in drug resistance in ovarian cancer. Wang *et al.* reported that PRDX3 protein expression is significantly higher in platinum-resistant ovarian cancer patients than in platinum-sensitive patients.[69] Recently, Duan *et al.* further demonstrated that downregulation of PRDX3 by siRNA enhanced cisplatin induced ovarian cancer cell apoptosis, providing new evidence of the potential application of PRDX3-siRNA in cancer therapy.[70] Regarding PRDX3 lung cancer, Kim *et al.* showed that PRDX3 was markedly overexpressed in human squamous cell carcinoma, suggesting that it may play a protective role against oxidative injury in lung cancer.[71] Our mRNA and protein level results confirm that PRDX3 expression is remarkably decreased in high metastatic lung cancer L9981 compared to low metastatic lung cancer NL9980 cell lines, indicating that PRDX3 might also be involved in the lung cancer metastatic process.

In summary, for the first time, we have identified mitochondrial differential expression profiling between lung
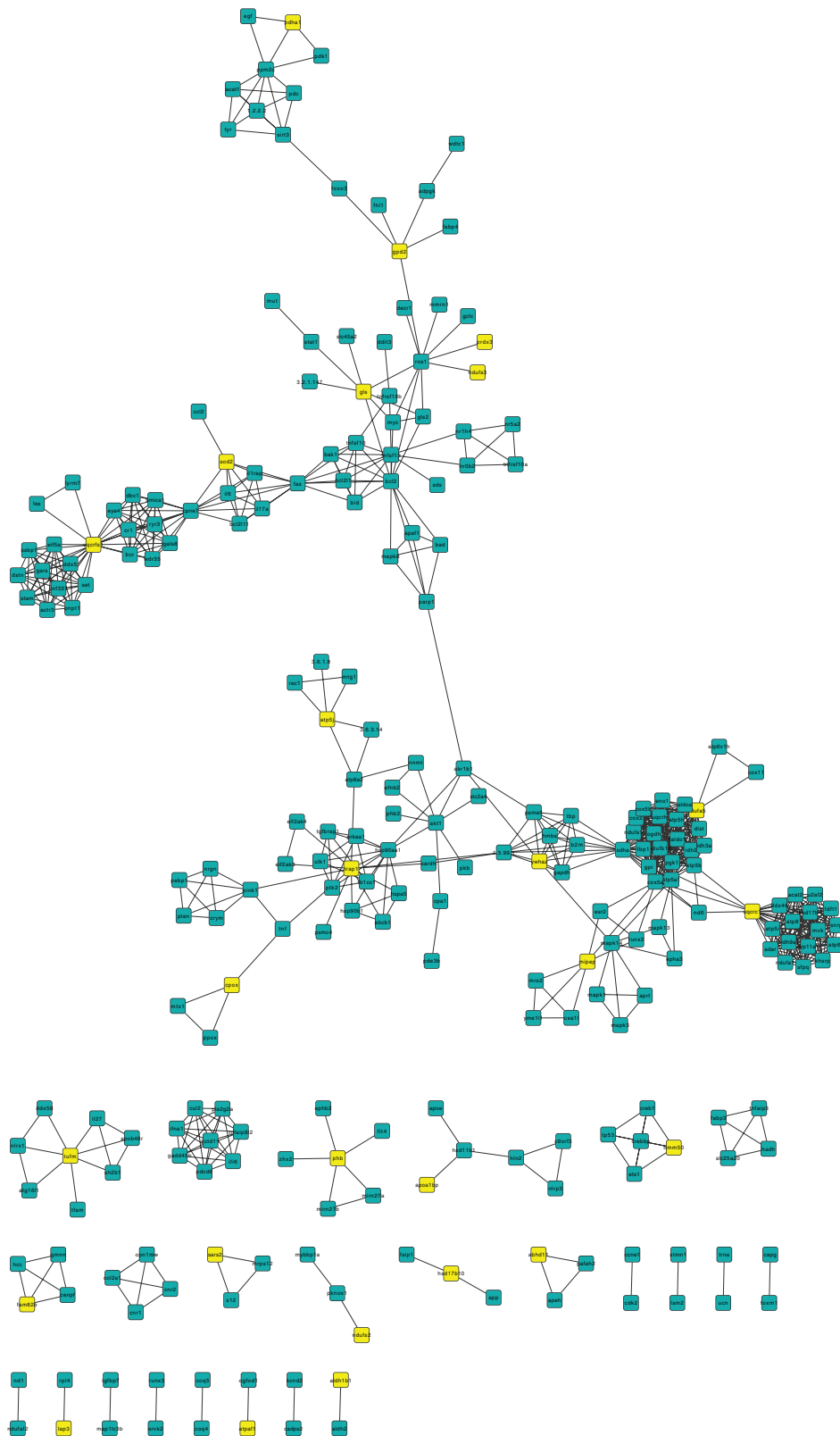
Figure 5 A protein–protein interaction subnetwork of differentially expressed mitochondrial proteins between NL9980 and L9981 cell lines with low and high metastatic potential. In this subnetwork, the colored circles (nodes) represent proteins, the yellow circles represent the proteins from our results, and the grey full lines (edges) represent protein–protein interactions.
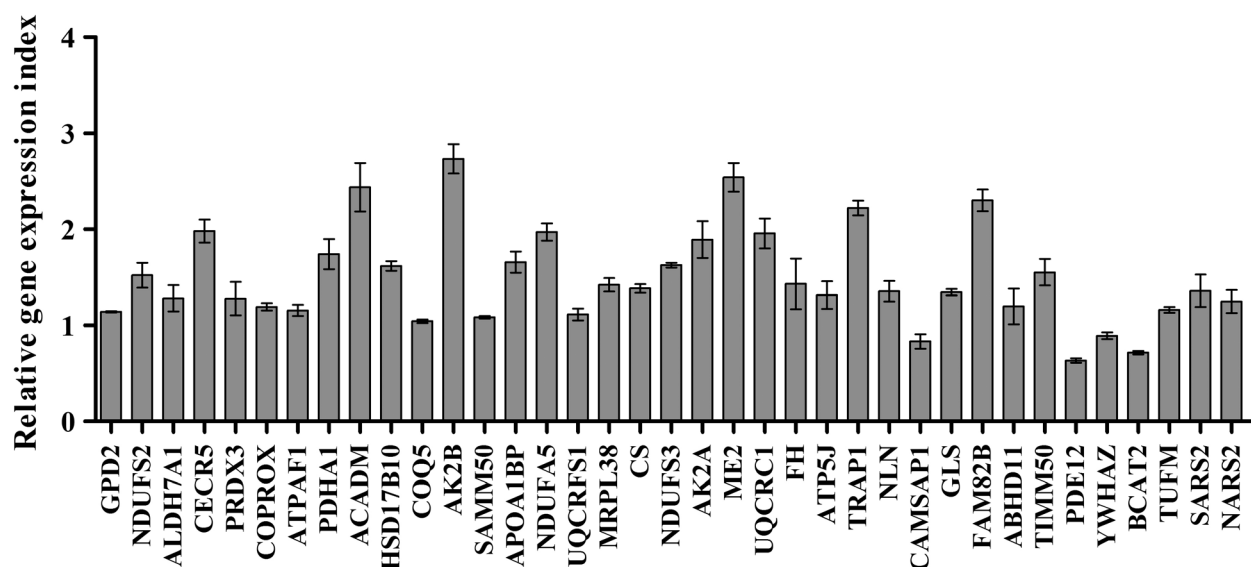
Figure 6 Real-time PCR analysis of differentially expressed mitochondrial proteins. After two-dimensional differential in gel electrophoresis analysis, 37 genes were further tested by real-time PCR. The relative gene expression of NL9980 cells compared to L9981 cells is shown.
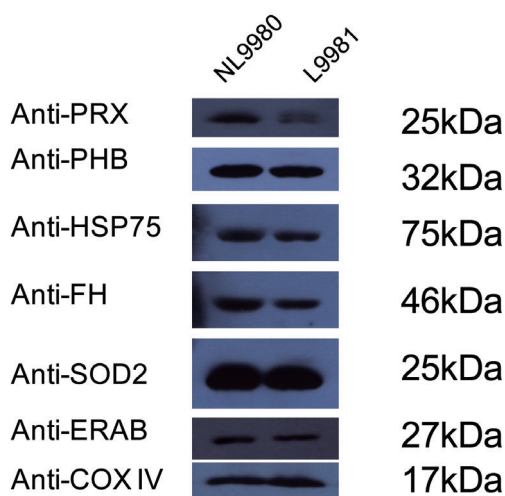

Figure 7 Validation of differentially expressed mitochondrial proteins by Western blot analysis. The expression of FH, PRDX3, HSP75, ERAB, and PHB proteins between NL9980 and L9981 cell lines were further validated by Western blot analysis. COX IV was used as an internal control for equal protein loading. One representative result out of three independent experiments is shown.

cancer cells with high and low metastatic potential by screening mitochondrial protein expression. Further investigation is necessary to determine the biological function and the relevance of the identified mitochondrial proteins in the metastatic process of lung cancer.

Disclosure

No authors report any conflict of interest.

References

1 Sun KX, Zheng RS, Zeng HM *et al.* [The incidence and mortality of lung cancer in China, 2014]. *Chin J Oncol* 2018, 23; **40** (11): 805–11 (In Chinese.).

2 Siegel RL, Miller KD, Jemal A. Cancer statistics, 2017. *CA Cancer J Clin* 2017; **67** (1): 7–30.

3 Chen W, Zheng R, Baade PD *et al.* Cancer statistics in China, 2015. *CA Cancer J Clin* 2015; **65** (1): 5–29.

4 Torre LA, Bray F, Siegel RL, Ferlay J, Lortet-Tieulent J, Jemal A. Global cancer statistics, 2012. *CA Cancer J Clin* 2015; **65** (2): 87–108.

5 Siegel RL, Miller KD, Jemal A. Cancer statistics, 2015. *CA Cancer J Clin* 2015; **65**: 5–29.

6 Siegel RL, Miller KD, Jemal A. Cancer statistics, 2016. *CA Cancer J Clin* 2016; **66** (1): 7–30. https://doi.org/10.3322/caac.21332.

7 Torre LA, Siegel RL, Ward EM, Jemal A. Global cancer incidence and mortality rates and trends--an update. *Cancer Epidemiol Biomarkers Prev* 2016; **25** (1): 16–27.

8 Wang JB, Fan YG, Jiang Y *et al.* Attributable causes of lung cancer incidence and mortality in China. *Thorac Cancer* 2011; **2** (4): 156–63.

9 Zheng R, Zeng H, Zuo T *et al.* Lung cancer incidence and mortality in China, 2011. *Thorac Cancer* 2016; **7** (1): 94–9.

10 Xu Y, Cao LQ, Jin LY *et al.* Quantitative proteomic study of human lung squamous carcinoma and normal bronchial epithelial acquired by laser capture microdissection. *J Biomed Biotechnol* 2012; **2012**: 510418.

11 Deng W, Yan M, Yu T *et al.* Quantitative proteomic analysis of the metastasis-inhibitory mechanism of miR-193a-3p in non small cell lung cancer. *Cell Physiol Biochem* 2015; **35**: 1677–88.

12 Cui YQ, Geng Q, Yu T *et al.* Establishment of a highly metastatic model with a newly isolated lung adenocarcinoma cell line. *Int J Oncol* 2015; **47**: 927–40.

13 Verschoor ML, Ungard R, Harbottle A, Jakupciak JP, Parr RL, Singh G. Mitochondria and cancer: Past, present, and future. *Biomed Res Int* 2013; **2013**: 612369.

14 Li W, Zhang X, Wang W *et al.* Quantitative proteomics analysis of mitochondrial proteins in lung adenocarcinomas and normal lung tissue using iTRAQ and tandem mass spectrometry. *Am J Transl Res* 2017; **9** (9): 3918–34.

15 Bustos G, Cruz P, Lovy A, Cárdenas C. Endoplasmic reticulum-mitochondria calcium communication and the regulation of mitochondrial metabolism in cancer: A novel potential target. *Front Oncol* 2017; **7**: 199.

16 Chen J-S, Chen K-T, Fan C-W *et al.* Comparison of membrane fraction proteomic profiles of normal and cancerous human colorectal tissues with gel-assisted digestion and iTRAQ labeling mass spectrometry. *FEBS J* 2010; **7** (14): 3028–38.

17 Liu Y, Lina B, Li W *et al.* Increased AAA-TOB3 correlates with lymph node metastasis and advanced stage of lung adenocarcinoma. *Int J Biol Markers* 2017; **32** (3): e325–32.

18 Yan B, Dong L, Neuzil J. Mitochondria: An intriguing target for killing tumour-initiating cells. *Mitochondrion* 2016; **26**: 86–93.

19 Tian L, Deng YT, Dong X *et al.* Siamese crocodile bile induces apoptosis in NCI-H1299 human non-small cell lung cancer cells via a mitochondria-mediated intrinsic pathway and inhibits tumorigenesis. *Mol Med Rep* 2017; **4**: 1727–37.

20 Che TF, Lin CW, Wu YY *et al.* Mitochondrial translocation of EGFR regulates mitochondria dynamics and promotes metastasis in NSCLC. *Oncotarget* 2015; **6** (35): 37349–66.

21 Yu C, Wang Y, Peng J *et al.* Mitochondrial calcium uniporter as a target of microRNA-340 and promoter of metastasis via enhancing the Warburg effect. *Oncotarget* 2017; **8** (48): 83831–44.

22 Li W, Zhang W, Deng W *et al.* Quantitative proteomic analysis of mitochondrial proteins differentially expressed between small cell lung cancer cells and normal human

bronchial epithelial cells. *Thorac Cancer* 2018; **9** (11): 1366–75.

23 Li Y, Zhou Q, Sun Z *et al.* [Experimental study on molecular mechanism of nm23-H1 gene transfection reversing the malignant phenotype of human high-metastatic large cell lung cancer cell line]. *Zhongguo Fei Ai Za Zhi* 2006; **9** (4): 307–11 (In Chinese.).

24 Steeg PS, Horak CE, Miller KD. Clinical-translational approaches to the Nm23- H1 metastasis suppressor. *Clin Cancer Res* 2008; **14** (16): 5006–12.

25 Marino N, Nakayama J, Collins JW, Steeg PS. Insights into the biology and prevention of tumor metastasis provided by the Nm23 metastasis suppressor gene. *Cancer Metastasis Rev* 2012; **31** (3–4): 593–603.

26 Che G, Chen J, Liu L *et al.* Transfection of nm23-H1 increased expression of beta-Catenin, E-Cadherin and TIMP-1 and decreased the expression of MMP-2, CD44v6 and VEGF and inhibited the metastatic potential of human non-small cell lung cancer cell line L9981. *Neoplasma* 2006; **53** (6): 530–7.

27 Marino N, Marshall JC, Collins JW *et al.* Nm23-h1 binds to gelsolin and inactivates its actin-severing capacity to promote tumor cell motility and metastasis. *Cancer Res* 2013; **73** (19): 5949–62.

28 Prabhu VV, Siddikuzzaman GVM, Guruvayoorappan C. Targeting tumor metastasis by regulating Nm23 gene expression. *Asian Pac J Cancer Prev* 2012; **13** (8): 3539–48.

29 Ma W, Chen J, Xue X *et al.* Alteration in gene expression profile and biological behavior in human lung cancer cell line NL9980 by nm23-H1 gene silencing. *Biochem Biophys Res Commun* 2008; **371** (3): 425–30.

30 Zhao R, Gong L, Li L *et al.* nm23-H1 is a negative regulator of TGF-β1-dependent induction of epithelial- mesenchymal transition. *Exp Cell Res* 2013; **319** (5): 740–9.

31 Yu F, Lu L, Zhihao W *et al.* nm23-H1 gene driven by hTERT promoter induce inhibition of invasive phenotype and metastasis of lung cancer xenograft in mice. *Thorac Cancer* 2013; **4** (1): 41–52.

32 Zhou QH, Yang XQ, Zhu DX *et al.* Double mutant P96S/S120Gof Nm23-H1 abrogates its NDPK activity and motility-suppressive ability. *Biochem Biophys Res Commun* 2007; **356** (2): 348–53.

33 Nie Q, Zhou QH, Zhu W *et al.* [nm23-H1 gene inhibits lung cancer cell invasion through down-regulation of PKC signal pathway]. *Chin J Oncol* 2006; **28** (5): 334–6 (In Chinese.).

34 Che GW, Zhou QH, Zhu W *et al.* [Molecular mechanism of reversing metastatic phenotype in human high-metastatic large cell lung cancer cell line L9981 by nm23-H1]. *Chin J Cancer* 2005; **24** (3): 278–84 (In Chinese.).

35 Zhou QH, Deng YL, Zhu W. Transfection of the metastatic suppressive gen nm23-H1 induce differential protein expression in human high-metastatic large cell lung cancer cell line L9981. *Mol Cell Proteomics* 2004; **3** (Suppl.10): S63.

36 Zhou QH, Zhu W, Deng YL. Preliminary analysis of two dimensional gel electrophoresis for proteomic of human

large cell lung cancer cell line before and after transfection of nm23-H1 gene. *Molecular & Cellular Proteomics* 2004; **3** (Suppl.10): S105.

37 Li Y, Zhou Q, Sun Z *et al.* [Transfection of the tumor metastasis suppressor gene nm23-H1 can targetly suppress the activity of extracellular signal-regulated protein kinase (ERK) in human high-metastasis large cell lung cancer cell line L9981]. *Zhongguo Fei Ai Za Zhi* 2004; **7** (1): 8–11 (In Chinese.).

38 Fu J, Zhou Q, Zhu W *et al.* [Effects of transfection of nm23-H1 gene on β-catenin expression in human high-metastatic large cell lung cancer cell line L9981]. *Zhongguo Fei Ai Za Zhi* 2004; **7** (6): 471–4 (In Chinese.).

39 Gong L, Wu Z, Guo L *et al.* Metastasis suppressor Nm23-H1 inhibits STAT3 signaling via a negative feedback mechanism. *Biochem Biophys Res Commun* 2013; **434** (3): 541–6.

40 Tang XJ, Zhou QH, Zhang SF, Liu LX. [Expressions of Nm23, E-cadherin, and beta-catenin in non-small cell lung cancer and their correlations with metastasis and prognosis.]. *Ai Zheng* 2005; **24** (5): 616–21 (In Chinese.).

41 Zhou Q, Wang Y, Che G *et al.* [Establishment and their biological characteristics of clonal cell subpopulations (NL9980 and L9981) from a human lung large cell carcinoma cell line (WCQH-9801).]. *Zhongguo Fei Ai Za Zhi* 2003; **6** (6): 464–8 (In Chinese.).

42 Carew JS, Huang P. Mitochondrial defects in cancer. *Mol Cancer* 2002; **1** (9): 1–12.

43 Hanahan D, Weinberg RA. Hallmarks of cancer: The next generation. *Cell* 2011; **144** (5): 646–74.

44 Chou HC, Chan HL. Targeting proteomics to investigate metastasis-associated mitochondrial proteins. *J Bioenerg Biomembr* 2012; **44** (6): 629–34.

45 Zhu W, Deng Y, Zhou Q *et al.* [Analysis of two-dimension gel electrophoresis of human large cell lung cancer cell lines with different metastasis potentials]. *Zhongguo Fei Ai Za Zhi* 2005; **8** (1): 1–7 (In Chinese.).

46 Ye Y, Huang A, Huang C *et al.* Comparative mitochondrial proteomic analysis of hepatocellular carcinoma from patients. *Proteomics Clin Appl* 2013; **7** (5–6): 403–15.

47 Liu J, Zhan X, Li M *et al.* Mitochondrial proteomics of nasopharyngeal carcinoma metastasis. *BMC Med Genomics* 2012; **5**: 62.

48 Park WS, Chung KW, Young MS, Kim SK, Lee YJ, Lee EK. Differential protein expression of lymph node metastases of papillary thyroid carcinoma harboring the BRAF mutation. *Anticancer Res* 2013; **33** (10): 4357–64.

49 Kiuru M, Launonen V. Hereditary leiomyomatosis and renal cell cancer (HLRCC). *Curr Mol Med* 2004; **4** (8): 869–75.

50 Yang Y, Lane AN, Ricketts CJ *et al.* Metabolic reprogramming for producing energy and reducing power in fumarate hydratase null cells from hereditary leiomyomatosis renal cell carcinoma. *PLoS One* 2013; **8** (8): e72179.

51 Linehan WM, Rouault TA. Molecular pathways: Fumarate hydratase-deficient kidney cancer: Targeting the Warburg effect in cancer. *Clin Cancer Res* 2013; **19** (13): 3345–52.

52 Sciacovelli M, Guzzo G, Morello V *et al.* The mitochondrial chaperone TRAP1 promotes neoplastic growth by inhibiting succinate dehydrogenase. *Cell Metab* 2013; **17** (6): 988–99.

53 Zhang L, Karsten P, Hamm S *et al.* TRAP1 rescues PINK1 loss-of-function phenotypes. *Hum Mol Genet* 2013; **22** (14): 2829–41.

54 Yoshida S, Tsutsumi S, Muhlebach G *et al.* Molecular chaperone TRAP1 regulates a metabolic switch between mitochondrial respiration and aerobic glycolysis. *Proc Natl Acad Sci U S A* 2013; **110** (17): E1604–12.

55 Agorreta J, Hu J, Liu D *et al.* TRAP1 regulates proliferation, mitochondrial function and has prognostic significance in NSCLC. *Mol Cancer Res* 2014; **12** (5): 660–9.

56 Liu D, Hu J, Agorreta J *et al.* Tumor necrosis factor receptor-associated protein 1 (TRAP1) regulates genes involved in cell cycle and metastases. *Cancer Lett* 2010; **296** (2): 194–205.

57 Caino MC, Chae YC, Vaira V *et al.* Metabolic stress regulates cytoskeletal dynamics and metastasis of cancer cells. *J Clin Invest* 2013; **123** (7): 2907–20.

58 Oppermann UC, Salim S, Tjernberg LO, Terenius L, Jörnvall H. Binding of amyloid beta-peptide to mitochondrial hydroxyacyl-CoA dehydrogenase (ERAB): Regulation of an SDR enzyme activity with implications for apoptosis in Alzheimer's disease. *FEBS Lett* 1999; **451** (3): 238–42.

59 Frackowiak J, Mazur-Kolecka B, Kaczmarski W, Dickson D. Deposition of Alzheimer's vascular amyloid-beta is associated with decreased expression of brain L-3-hydroxyacyl-coenzyme A dehydrogenase (ERAB). *Brain Res* 2001; **907** (1–2): 44–53.

60 Shen LY, Chen KN. Exploration of target genes of HOXA13 in esophageal squamous cell carcinoma cell line. *Cancer Lett* 2011; **312** (1): 18–23.

61 Coates PJNR, McGregor A, Picksley SM, Crouch DH, Hall PA. Mammalian prohibitin proteins respond to mitochondrial stress and decrease during cellular senescence. *Exp Cell Res* 2001; **265** (2): 262–73.

62 Sripathi SRHW, Atkinson CL *et al.* Mitochondrialnuclear communication by prohibitin shuttling under oxidative stress. *Biochemistry* 2011; **50** (39): 8342–51.

63 Dart DA, Spencer-Dene B, Gamble SC, Waxman J, Bevan CL. Manipulating prohibitin levels provides evidence for an in vivo role in androgen regulation of prostate tumors. *Endocr Relat Cancer* 2009; **16** (4): 1157–69.

64 Liu X, Ren Z, Zhan R *et al.* Prohibitin protects against oxidative stress-induced cell injury in cultured neonatal cardiomyocyte. *Cell Stress Chaperones* 2009; **14** (3): 311–9.

65 Ko KS, Tomasi ML, Iglesias-Ara A *et al.* Liver-specific deletion of prohibitin 1 results in spontaneous liver injury,

fibrosis, and hepatocellular carcinoma in mice. *Hepatology* 2010; **52** (6): 2096–108.

66 Rajalingam K, Wunder C, Brinkmann V *et al.* Prohibitin is required for Ras-induced Raf-MEK-ERK activation and epithelial cell migration. *Nat Cell Biol* 2005; **7** (8): 837–43.

67 Basu A, Banerjee H, Rojas H *et al.* Differential expression of peroxiredoxins in prostate cancer: Consistent upregulation of PRDX3 and PRDX4. *Prostate* 2011; **71** (7): 755–65.

68 Whitaker HC, Patel D, Howat WJ *et al.* Peroxiredoxin-3 is overexpressed in prostate cancer and promotes cancer cell survival by protecting cells from oxidative stress. *Br J Cancer* 2013; **109** (4): 983–93.

69 Wang XY, Wang HJ, Li XQ. Peroxiredoxin III protein expression is associated with platinum resistance in epithelial ovarian cancer. *Tumour Biol* 2013; **34** (4): 2275–81.

70 Duan J, Lang Y, Song C, Xiong J, Wang Y, Yan Y. siRNA targeting of PRDX3 enhances cisplatin-induced apoptosis in ovarian cancer cells through the suppression of the NF-κB signaling pathway. *Mol Med Rep* 2013; **7** (5): 1688–94.

71 Kim YS, Lee HL, Lee KB *et al.* Nuclear factor E2-related factor 2 dependent overexpression of sulfiredoxin and peroxiredoxin III in human lung cancer. *Korean J Intern Med* 2011; **26** (3): 304–13.